

# Simplified Solution for Periodic Thermal Discontinuities in Asphalt Overlays Bonded to Rigid Pavements

H. M. Yin<sup>1</sup>; W. G. Buttlar, M.ASCE<sup>2</sup>; and G. H. Paulino, M.ASCE<sup>3</sup>

**Abstract:** This work investigates the elastic fields which develop in an overlay bonded to a rigid substrate when the system is subjected to thermally induced stress. A two-dimensional solution of the displacement field is derived for periodic discontinuities distributed in a hot mix asphalt overlay bonded to a rigid pavement, where the length of the pavement before cracking develops is much larger than its layer thickness. A series form solution is obtained, requiring calibration due to the limitation of the basis functions used. The formulation allows thermal cracks of variable depth to be considered, and its accuracy is verified through comparisons with numerical solutions obtained with ABAQUS. Energy release rates are calculated from the model for top-down plane strain cracking and three-dimensional channeling. By comparing the energy release rates with the fracture toughness of the overlay, conditions for crack initiation and an estimation of crack depth for a given temperature change can be estimated. Although several simplifying assumptions are made in the current approach, it is shown to be more general and therefore more widely applicable as compared to existing closed-form solutions. The solutions are valuable to the pavement analyst who seeks to understand the general mechanisms of thermally induced pavement deterioration and for the researcher wishing to perform early stage verification of more complex pavement models.

**DOI:** 10.1061/(ASCE)0733-947X(2007)133:1(39)

**CE Database subject headings:** Thermal stresses; Fracture mechanics; Asphalt pavements; Rigid pavements; Cracking.

## Introduction

A concrete pavement which has been rehabilitated with an asphalt overlay can be generally described as an overlay/substrate system (Bozkurt 2002; Bozkurt and Buttlar 2002; Kim and Buttlar 2002). These systems are also common in the electronic packaging and protective coating industries, as described by Hutchinson and Suo (1992), Freund and Suresh (2003), Huang et al. (2003), and Zhang and Huan (2004). When these systems are subjected to an ambient temperature change, thermal cracking may initiate on the overlay surface and propagate toward the interface, often with a uniform crack spacing pattern (Shenoy et al. 2001), and occasionally with very devastating effects [Figs. 1(a and b)]. Advances in design and maintenance of these material systems require the direct consideration of material discontinuities as part of the structural analysis process.

Hot mix asphalt (HMA) pavements are typically overlay/substrate systems with one or more asphalt concrete layers con-

structed upon either: granular aggregate layers; compacted soil layers (sometimes cement- or pozzolanically stabilized), or, in case of pavement rehabilitation; existing Portland cement concrete slabs. Various empirical and “mechanistic-empirical” models (Fromm and Phang 1972; Hass et al. 1987; Roque et al. 1995) have been proposed, in which various field observations and laboratory experiments were conducted to predict crack spacing in asphalt pavements.

One of the most popular applications of HMA overlays is in the rehabilitation of Portland cement concrete (PCC) pavements. PCC pavements can be classified into four types: jointed plain concrete pavement (JPCP), jointed reinforced concrete pavement (JRCP), continuous reinforced concrete pavement (CRCP), and prestressed concrete pavement (PCP) (Huang 2003). When HMA surfaces are laid over CRCP and PCP base courses, thermal cracking is the primary contributor to the transverse cracking of HMA surfaces in cold climates. Another contributor to transverse cracking of HMA surfaces is reflective cracking, which is especially prevalent in JPCP and JRCP pavements with shorter joint spacing [Fig. 1(a)]. Since reflective cracks often occur more rapidly than thermal cracks, a thermal cracking analysis in this case may be of secondary importance. Furthermore, frequent reflective cracks would tend to limit the amount of tensile stress available for thermal crack development between these cracks. However, for JRCP pavements with longer joint spacing (over 15 m), and for CRCP and PCP pavements, where slab length is much larger than the width of the pavements, transverse thermal cracks may develop between existing reflective cracks and may represent a major form of overlay deterioration in cold climates [Fig. 1(b)].

This work studies low temperature cracking in PCC pavements with HMA overlays, particularly JRCP pavements with longer joint spacing (greater than 15 m), CRCP and PCP, where the PCC layer is relatively stiff compared to the HMA overlay. As

<sup>1</sup>Transportation Engineer, Office of Flexible Pavement Materials, Transportation Laboratory, 5900 Folsom Blvd., Sacramento, CA 95833 (corresponding author). E-mail: huiming\_yin@dot.ca.gov

<sup>2</sup>Associate Professor, Dept. of Civil and Environmental Engineering, Univ. of Illinois at Urbana-Champaign, 1212 Newmark Civil Engineering Laboratory, 205 N. Mathews Ave., Urbana, IL 61801.

<sup>3</sup>Professor, Dept. of Civil and Environmental Engineering, Univ. of Illinois at Urbana-Champaign, 2209 Newmark Civil Engineering Laboratory, 205 N. Mathews Ave., Urbana, IL 61801.

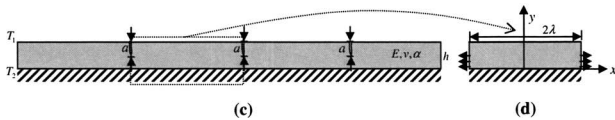
Note. Discussion open until June 1, 2007. Separate discussions must be submitted for individual papers. To extend the closing date by one month, a written request must be filed with the ASCE Managing Editor. The manuscript for this paper was submitted for review and possible publication on December 27, 2005; approved on June 5, 2006. This paper is part of the *Journal of Transportation Engineering*, Vol. 133, No. 1, January 1, 2007. ©ASCE, ISSN 0733-947X/2007/1-39-46/\$25.00.



(a)



(b)



(c)

(d)

**Fig. 1.** Asphalt overlay bonded to rigid substrate with nearly uniformly distributed cracks: (a) field observation of asphalt pavement with sealed reflective cracks (right lane); (b) field observation of asphalt pavement with thermal cracks (left lane); (c) elevation view of pavement model with periodic discontinuities; and (d) typical section between two cracks

seen in Fig. 1(b), these asphalt surfaces may undergo thermal cracking after several winters, particularly in very cold climates. With the decrease of temperature, the asphalt overlay undergoes contractive deformation, inducing tensile stress. When the strain energy in the asphalt overlay reaches a value that it is higher than fracture toughness (i.e., maximum fracture resistance) of the asphalt material, transverse cracks may initiate at the surface and propagate across the width and through the depth of the pavement, often with roughly uniform (periodic) crack spacing. During crack initiation and propagation, strain energy is dissipated as fracture energy, such that tensile stress in the overlay in the vicinity of the crack is relieved. With the further decrease of temperature, new cracks may continuously initiate in a similar manner.

Although the aforementioned empirical models have been shown to provide reasonable predictions of crack spacing in asphalt pavements, the thermal stress distribution in pavements, a dominant factor controlling thermal crack development, has not been directly investigated in those models. To analyze the elastic fields of pavements, the finite-element method has been widely

used to calculate the local stress and strain (Yang and Lin 1995; Shalaby et al. 1996; Davids and Turkiyyah 1997; Waldhoff et al. 2000). Since the quality of numerical simulations depends on the quality of meshing (e.g. discretization aspects), it is not straightforward to extend the results to general cases. Thus, analytical solutions are a valuable tool for researchers for model verification, and ultimately, to gain a better insight into mechanical responses and damage mechanisms in pavements.

Shen and Kirkner (1999), Timm et al. (2003), and Chen and Baker (2004), respectively, developed a one-dimensional (1D) model to predict tensile stress distribution in a pavement with frictional constraint. The frictional force from the substrate is balanced by a uniform tensile stress along the thickness of the overlay. Because the frictional forces reside at the bottom of the pavement, considerable shear stress will be induced along the bottom of the overlay, but vanishes along the free surface. Since a 1D model can neither solve the shear stress distribution in the overlay nor consider the temperature field along the thickness, a two-dimensional (2D) model is necessary to accurately describe the thermal stress distribution.

Beuth (1992) presented solutions for fully and partially cracked film problems for elastic films bonded to elastic substrates with one crack and showed that when an overlay is fully bonded to a rigid substrate, the crack tips will stop within the overlay. Hong et al. (1997) developed a model to predict the crack spacing and crack depth in highway pavements assuming that the effect of a crack in the overlay could be described by an increase in effective compliance. Xia and Hutchinson (2000) and Shenoy et al. (2001), respectively, investigated crack patterns in overlays and proposed an elastic solution in the integral form using dislocation solutions as the weight functions in the integrals, namely, kernel functions.

Yin et al. (2005) presented an explicit elastic solution for an overlay resting on a granular base considering frictional boundary condition and fully thermal discontinuities. In this paper, we will investigate the elastic fields due to partial-depth cracks in a HMA overlay bonded to a rigid pavement and subjected to a temperature change. When an HMA overlay is placed on a PCC pavement, the HMA is more compliant than the substrate and thus the substrate can be modeled as perfectly rigid. At low temperatures, the HMA can be approximated as linear elastic. The purpose of this study is to model existing thermally induced transverse cracks, initiated at the free surface and periodically distributed. Other discontinuities, such as reflective cracks and fatigue cracks are not considered in the current study.

During the derivation, the general solution for the displacement field is derived for the 2D overlay in a series form, which is calibrated using the crack opening displacement on the overlay surface. The convergence characteristics of the solution is then presented. Comparisons of the solution with those obtained by finite-element simulations are presented, which demonstrate the accuracy of the proposed model. Using this solution, one can easily calculate the energy release rates for top-down plane strain cracking and three-dimensional (3D) channeling, which propagates transverse to the direction of traffic. Comparing the energy release rates with the fracture toughness of the overlay, one can predict the crack depth and likelihood for crack initiation under given temperature change.

## Formulation

Consider an infinitely long overlay (thickness  $h$ , Young's modulus  $E$ , and Poisson's ratio  $\nu$ ) resting on a rigid substrate, which is

subjected to an ambient temperature change  $T$ , as illustrated in Fig. 1(c). Because the overlay and the substrate have different thermal expansion coefficients, whose difference is defined as  $\alpha = \alpha_{\text{film}} - \alpha_{\text{substrate}}$ , a residual stress is induced in the overlay as

$$\sigma_0 = -\frac{E}{1-\nu}\alpha T \quad (1)$$

Here the plane strain condition is considered for the overlay subjected to isotropic thermal strain. In this paper, only the tensile stress, i.e.,  $\sigma_0 > 0$ , is considered. The thermal strain of the substrate can be simply disregarded by treating it as a perfectly rigid body. With the increase of  $\sigma_0$ , uniformly spaced discontinuities with spacing of  $2\lambda$  will form in the overlay and the stress will be redistributed. For a compliant overlay on a rigid substrate, cracks may not cross the full depth of the overlay, and the crack tips stop within the overlay (Beuth 1992). Here the length of the discontinuities is denoted as  $a$ . Assuming a periodic boundary condition, identical elastic fields will reside in each section between discontinuities. Considering the marked section, one can set up the coordinates with the origin at the center of the bottom of the overlay as seen in Fig. 1(d).

The overlay is assumed to be fully bonded to the rigid substrate and the bottom of the overlay is assumed to remain in plane. Because the thickness of the overlay is much smaller than its length, the top surface is free, and assuming that no debonding occurs along the interface between the overlay and the substrate, the top surface of the overlay is also assumed to remain in plain during temperature changes. Thus, it is assumed that all points of a plane normal to the  $y$  direction remain the same plane after deformation, i.e.

$$u_y(x, y) = u_y(y) \quad (2)$$

Because the upper surface is free, the thermal strain in the  $y$  direction is not constrained. Thus, it is assumed that the stress in the  $y$  direction is zero, i.e.

$$\sigma_y(x, y) = 0 \quad (3)$$

For this plane strain problem, the constitutive relation reads

$$\sigma_x = \bar{E}\varepsilon_x + \sigma_0, \quad \tau_{xy} = \mu\gamma_{xy} \quad (4)$$

where

$$\bar{E} = E/(1-\nu^2), \quad \mu = E/[2(1+\nu)] \quad (5)$$

and

$$\varepsilon_x = u_{x,x}, \quad \gamma_{xy} = u_{x,y} \quad (6)$$

Here  $u_{y,x} = 0$  is used to solve for  $\gamma_{xy}$ . Considering the equilibrium condition in  $x$  direction, one can write

$$Eu_{x,xx} + \mu u_{x,yy} = 0 \quad (7)$$

Using the method of separation of variables, one can obtain the general solution as

$$u_x(x, y) = (A_1 e^{cx/h} + A_2 e^{-cx/h})[B_1 \sin(dy/h) + B_2 \cos(dy/h)] \quad (8)$$

where coefficients  $A_1$ ,  $A_2$ ,  $B_1$ , and  $B_2$  will be decided by the boundary conditions and  $d = \sqrt{\bar{E}/\mu c}$ .

From the symmetry of the geometry and the free upper surface, it is written

$$u_x(0, y) = 0; \quad u_{x,y}(x, h) = 0 \quad (9)$$

Using the above boundary conditions, one can simplify Eq. (8) as

$$u_x(x, y) = B \sinh(cx/h) \cos[d(1-y/h)] \quad (10)$$

Along the bottom of the overlay, the displacement is fixed due to the rigid substrate, i.e.

$$u_x(x, 0) = 0 \quad (11)$$

Substituting Eq. (10) into Eq. (11), one can derive

$$d_i = i\pi - \frac{\pi}{2}; \quad c_i = \sqrt{\mu/\bar{E}}d_i \quad (12)$$

with  $i = 1, 2, \dots$ . Then, the displacement field is written as

$$u_x(x, y) = \sum_{i=1}^N B_i \sinh(c_i x/h) \cos[d_i(1-y/h)] \quad (13)$$

Here  $N$  can be a large number, whose value depends on the convergence of the solution, which will be discussed later; and  $B_i$  ( $i = 1, 2, \dots, N$ ) is the displacement component corresponding to the basis function. Considering the boundary condition of the end, one can know that the tensile stress above the discontinuity tip is zero due to the free surface and that the displacement field under the discontinuity tip is zero due to the symmetric boundary condition, which yields the following:

$$\sum_{i=1}^N B_i c_i \cosh(c_i \lambda/h) \cos[d_i(1-y/h)] + \frac{h\sigma_0}{\bar{E}} = 0, \quad \text{for } h-a \leq y \leq h \quad (14)$$

and

$$\sum_{i=1}^N B_i \sinh(c_i \lambda/h) \cos[d_i(1-y/h)] = 0, \quad \text{for } 0 \leq y < h-a \quad (15)$$

This boundary condition cannot be rigorously satisfied at every point by a selection of a finite number of functions in Eq. (13). Here a piecewise function is defined to describe the error as

$$e(y) = \begin{cases} \sum_{i=1}^N B_i c_i \cosh(c_i \lambda/h) \cos[d_i(1-y/h)] + \frac{h\sigma_0}{\bar{E}} & h-a \leq y \leq h \\ \sum_{i=1}^N B_i \sinh(c_i \lambda/h) \cos[d_i(1-y/h)] & 0 \leq y < h-a \end{cases} \quad (16)$$

Since there are  $N$  unknowns as  $B_i$ ,  $N$  weight functions are used to establish weighted residual equations posed as follows:

$$\int_0^h e(y) \cos[d_i(1-y/h)] dy = 0, \quad i = 1, 2, \dots, N \quad (17)$$

From the above  $N$  equations, one can solve for  $B_i$ . Substitution of Eq. (16) into Eq. (17) provides

$$A_{ij} B_j = f_i \quad (18)$$

where

$$f_i = - \int_{h-a}^h \frac{h\sigma_0}{\bar{E}} \cos[d_i(1-y/h)] dy = - \frac{h^2 \sigma_0}{\bar{E} d_i} \sin \frac{d_i a}{h} \quad (19)$$

and

$$A_{ij} = \int_{h-a}^h c_j \cosh(c_j \lambda / h) \cos[d_j(1-y/h)] \cos[d_i(1-y/h)] dy + \int_0^{h-a} \sinh(c_j \lambda / h) \cos[d_j(1-y/h)] \cos[d_i(1-y/h)] dy \quad (20)$$

For  $i \neq j$ ,  $A_{ij}$  is given by

$$A_{ij} = \frac{1}{2} \left[ \frac{h}{d_i - d_j} \sin \frac{(d_i - d_j)a}{h} + \frac{h}{d_i + d_j} \sin \frac{(d_i + d_j)a}{h} \right] \times \left[ c_j \cosh \left( \frac{c_j \lambda}{h} \right) - \sinh \left( \frac{c_j \lambda}{h} \right) \right]$$

and for  $i = j$ ,  $A_{ij}$  is given by

$$A_{ij} = \frac{ac_j}{2} \cosh \left( \frac{c_j \lambda}{h} \right) + \frac{h-a}{2} \sinh \left( \frac{c_j \lambda}{h} \right) + \frac{h}{4d_i} \sin \frac{2d_i a}{h} \left[ c_j \cosh \left( \frac{c_j \lambda}{h} \right) - \sinh \left( \frac{c_j \lambda}{h} \right) \right]$$

From Eq. (18),  $B_i$  can be determined, after which the displacement field in Eq. (13) can be obtained, from which the stress fields can easily be derived as

$$\sigma_x = \sum_{i=1}^N \frac{\bar{E} B_i c_i}{h} \cosh(c_i x / h) \cos[d_i(1-y/h)] + \sigma_0 \quad (21)$$

and

$$\tau_{xy} = \sum_{i=1}^N \mu \frac{B_i d_i}{h} \sinh(c_i x / h) \sin[d_i(1-y/h)] \quad (22)$$

Because the error function in Eq. (16) is piecewise, and the two assumptions of Eqs. (2) and (3) are used, the series form solution with a limited number of basis functions in Eq. (13) may not approach the exact solution. The convergence and accuracy of the solution are explored in the following section.

## Convergence and Calibration

To show the convergence of the proposed solution, the displacement field changing with the discontinuity spacing and discontinuity depth is investigated when using a finite number of functions in Eq. (13). In the numerical simulations,  $\nu=0.2$  and  $h=1$  are used. Fig. 2 shows the displacement field distribution along the cracked end for  $\lambda/h=4.0$ . In Fig. 2(a), the overlay is fully cracked. Notice that when  $N=3$  the results are very close to those obtained for  $N=10$ , which indicates that the solution converges very rapidly. However, for a partial-depth crack with  $a/h=0.4$ , Fig. 2(b) shows that the solution converges more slowly. When  $N$  is large, the displacement under the crack tip will converge to zero, although the rate of convergence is slow. As a minimal requirement, it is suggested to let  $N > h/(2a) + 1$  so that the piecewise boundary condition along the cracked end will be minimally embodied. For instance, in the case of the example shown in Fig. 2(b), the minimal requirement is  $N > 2.25$ . The curve for  $N=1$  ( $N < 3$ ), which is a monotonically decreasing function, cannot illustrate the piecewise boundary condition with a connection point at  $y=0.6$ . Fig. 2(c) shows the displacement field distribution along the fully cracked end for a smaller crack spacing

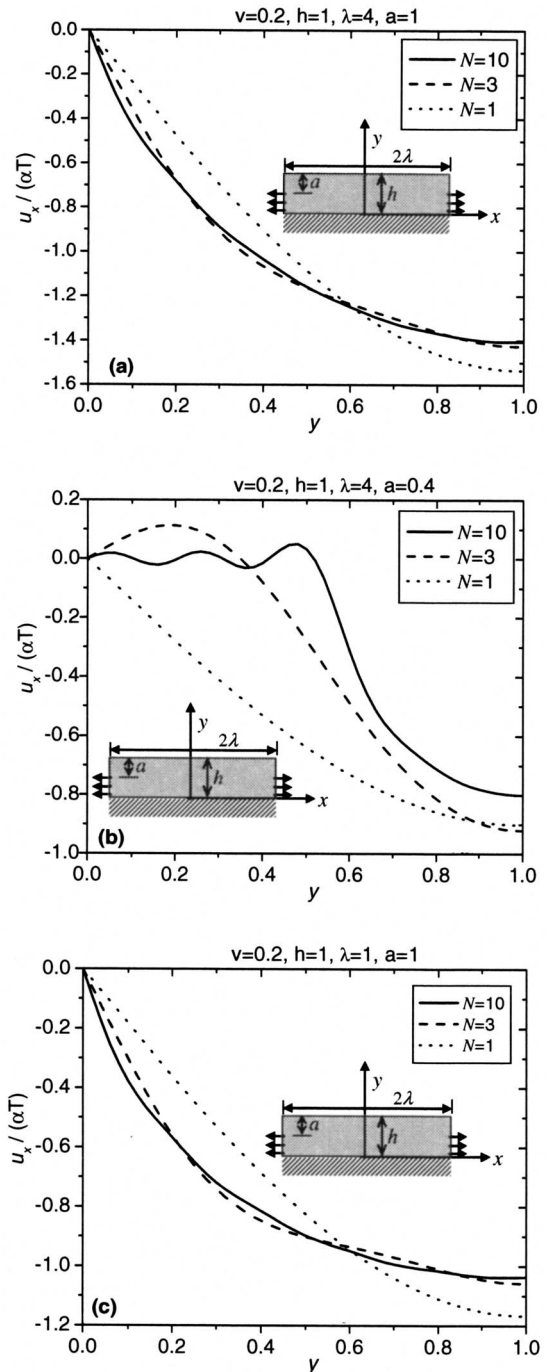


**Fig. 2.** Convergence of the solution as a function of crack depth and crack spacing: (a)  $a=h$ ;  $\lambda=4h$ ; (b)  $a=0.4h$ ;  $\lambda=4h$ ; and (c)  $a=h$ ;  $\lambda=h$

ing ( $\lambda/h=1.0$ ). It can be observed that the convergence speed is somewhat slower than that for  $\lambda/h=4.0$  in Fig. 2(a) but the difference is relatively small. Thus, the crack spacing only has a minor effect on the rate of convergence.

Fig. 3 illustrates the convergence of the solution along the boundary condition. The results for normalized discontinuity depths  $a/h=1, 0.6$ , and  $0.2$  are presented. A large number of functions are used as  $N=80$ . The thicker curves show the solutions from Eqs. (13) and (21), whereas the thinner curves with circles represent the calibrated results, which will be elaborated upon later. In Fig. 3(a), the displacement field under the discontinuity

The thinner curves with circles denote the calibrated results.

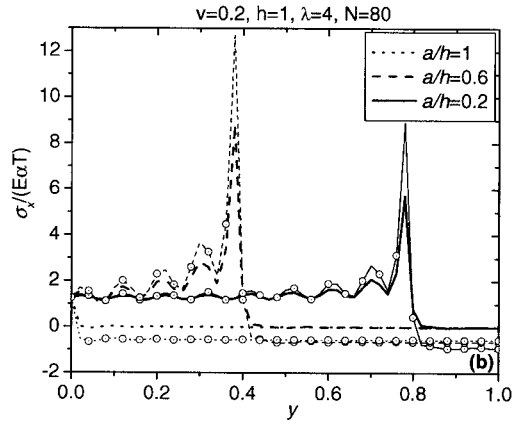
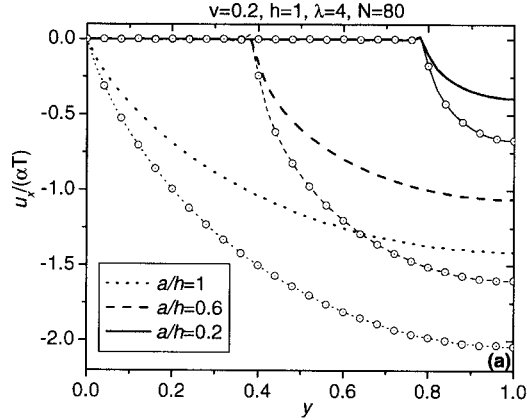


**Fig. 3.** Elastic fields along cracked end: (a) displacement field; (b) stress field. Thicker curves represent original modeling results; thinner curves with circles represent calibrated results.

tip is apparently zero but that above the discontinuity tip is negative; whereas, in Fig. 3(b), the stress along the cracked surface is zero but that under the discontinuity tip is tensile as predicted. In addition, in Fig. 3(b), it can be observed that the stress is very high in the neighborhood of the discontinuity tip due to the singularity at the discontinuity tip. However, a nonphysical fluctuation of the stress under the discontinuity tip is also seen in Fig. 3(b). This is a result of the fact that the assumptions in Eqs. (2) and (3) cannot be exactly satisfied, and thus the stress distribution cannot be exactly described by the set of the basis functions in Eq. (13). To calibrate this model, one can construct a multiplier  $k$  on all of the displacement components  $B_i$  by normalizing the crack mouth opening displacement (CMOD) on the overlay surface. Then the actual displacement components are written as

$$\bar{B}_i = kB_i \quad (23)$$

From Eq. (13), one can write CMOD as

$$\delta(a) = \sum_{i=1}^N 2kB_i \sinh(c_i \lambda/h) \quad (24)$$

Shenoy et al. (2001) showed that when the crack spacing is larger than five times of the thickness of the overlay, i.e.,  $\lambda/h > 2.5$ , the effect of the crack spacing on CMOD can be disregarded. Fitting the curve for  $\alpha = -0.99$  and  $\lambda/h > 2.5$  given by Shenoy et al. (2001), one can obtain the CMOD as

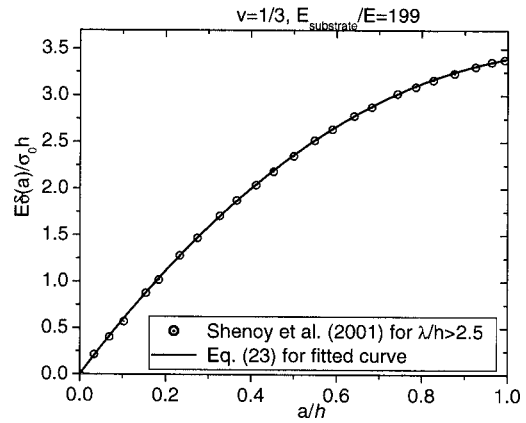


**Fig. 4.** Normalized crack opening displacement on overlay surface as function of crack depth  $a/h$

$$\delta(a) = 0.2456 \left( \frac{a}{h} \right) \left( \frac{a}{h} - 2.574 \right) \left( \frac{a}{h} - 9.777 \right) \frac{h\sigma_0}{E} \quad (25)$$

Fig. 4 illustrates the comparisons of the fitted function with the data presented by Shenoy et al. (2001). It is noted that the above equation is approximately obtained for  $\nu = 1/3$  and  $E_{\text{substrate}}/E = 199$  (Shenoy et al. 2001). Clearly, the substrate is so much stiffer than the overlay that it can be assumed as rigid. Beuth (1992) and Xia and Hutchinson (2000) showed that Poisson's ratio has only a minor effect and can be disregarded. Comparing Eq. (24) with Eq. (25), one can obtain

$$k = -0.1228 \left( \frac{a}{h} \right) \left( \frac{a}{h} - 2.574 \right) \left( \frac{a}{h} - 9.777 \right) \frac{h\sigma_0}{E \sum_{i=1}^N B_i \sinh(c_i \lambda/h)} \quad (26)$$

Substituting Eqs. (23) into (13), one can find that the calibrated solution not only satisfies the displacement boundary condition under the discontinuity tip as zero but also provides an accurate displacement for CMOD. Thus, this calibrated solution will give a good prediction of the displacement field. In Fig. 3(a), the calibrated results are of higher value than the original modeling results for all the three depths. However, a nonzero stress along the cracked free surface is produced due to this calibration. In Fig. 3(b), it is seen that along the cracked surface, the tensile stresses are constant but different for the three depths.

## Model Verification and Discussion

To verify the proposed model, comparisons are made with the finite-element method (FEM) simulations by *ABAQUS*. Due to the symmetry of the problem, only half of the section is modeled, using 10,890 four-node quadrilateral elements under plane strain conditions. The mesh and the boundary condition are shown in Fig. 5. In the numerical simulation, the following parameters are used:  $\nu = 0.2$ ;  $h = 1$ ; and  $\lambda = 4$ .

Because thermal cracks are generally assumed to initiate at the surface, Fig. 6 presents a comparison of the proposed prediction with the FEM simulation results for elastic fields along the surface of the overlay for different crack depths. The following features can be observed:

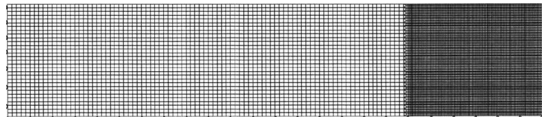


**Fig. 5.** Finite-element mesh used to model half of section between two cracks. Bottom nodes are fixed, while  $x$ -directional displacements along the two ends are constrained, except for the cracked, free surface.

- In Fig. 6(a), the displacement field is zero at the symmetric point, decreases along with  $x$ , and reaches the minimum at the cracked end. The proposed model is in good agreement with the FEM results.
- For the full crack with  $a/h=1$  in Fig. 6(b), the stress on the surface of the overlay monotonically decreases along with  $x$  and reaches the minimum with negative values at the cracked end. The proposed model is in good agreement with the FEM results.
- For the partial-depth crack with  $a/h=0.6$  or  $0.2$  in Fig. 6(b), the proposed predictions of the tensile stress along the surface still monotonically decrease with  $x$ ; whereas the FEM results reach a minimum at a peak point and then increase to zero at the end. The proposed model cannot capture the nonmonotonic tendency in the neighborhood of the cracked end, but nevertheless matches well with the FEM results in the region of highest tensile stress, which is of primary interest in analyzing crack spacing.

In the neighborhood of the crack tip, because the basis function in Eq. (13) does not reflect the inflection point of the stress distribution, it is impossible to find a solution from the set of basis functions that both satisfies the stress boundary condition and provides a good prediction for the displacement field. Using the calibration in Eq. (23), one can obtain a good agreement with FEM results for the displacement field but the stress-free boundary condition is not exactly satisfied at the cracked end. In summary, for the case where response away from the free end is needed, i.e., for determining crack spacing, this method works very well. However, for the case where the stress distribution close to the discontinuity is desired, this solution is not recommended.

With an increase of the thermal loading, a crack will initiate at a flaw on the surface of the overlay and would be expected to propagate in two modes: top-down plane strain cracking toward the interface and 3D channeling across the overlay, as illustrated in Figs. 7(a) and 7(b), respectively. For plane strain cracking, using Eqs. (13), (21), and (22) with the calibrated displacement components in Eq. (23), one can obtain the elastic fields in the section of the overlay. Considering the periodic distribution of the elastic fields in Fig. 1(b), one can expand the solution of the section to all other sections, and then calculate the path-independent  $\mathbf{J}$  integral along a counterclockwise contour line. For instance, it is computed along a line with four segments as seen in Fig. 7(a):  $S_1: y=0$  and  $x$  is from  $0$  to  $2\lambda$ ;  $S_2: x=2\lambda$  and  $y$  is from  $0$  to  $h$ ;  $S_3: y=h$  and  $x$  is from  $2\lambda$  to  $0$ ; and  $S_4: x=0$  and  $y$  is from  $h$  to  $0$ . Thus, the energy release rate for top-down plane strain cracking is calculated. For 3D channeling, the energy release rate can be calculated as the work done to close the crack opening displacement for unit length of the channeling advance. For a given crack depth, if  $\sigma_x^0$  is applied along the crack surface, it can be exactly closed. Therefore, the energy release rate (Beuth 1992) can be written as

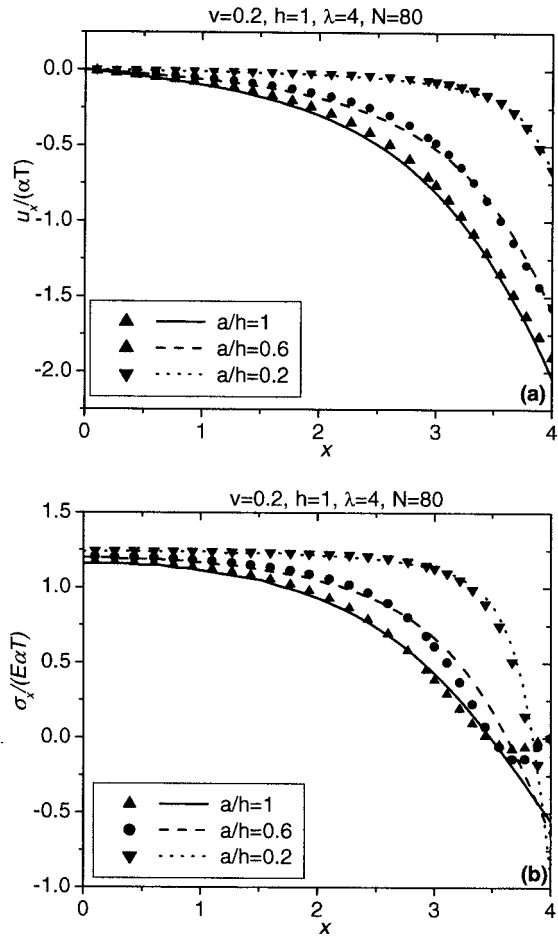


**Fig. 6.** Comparisons of elastic fields along top of overlay: (a) displacement field; (b) stress field. Symbols denote FEM results; curves represent closed-form solutions.

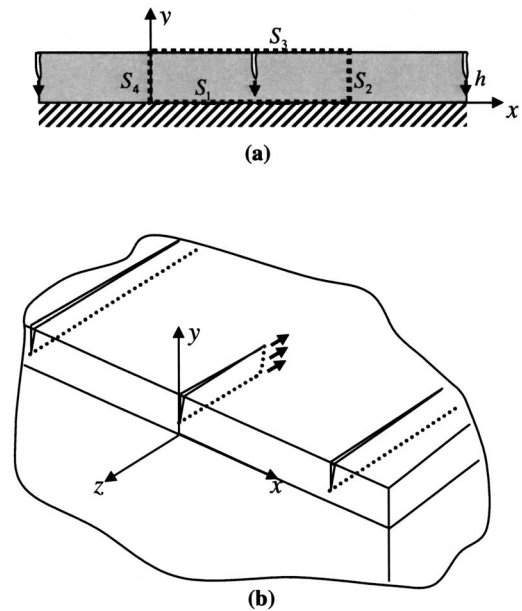


**Fig. 7.** Schematic illustration of thermal cracking in asphalt overlays: (a) top-down plane strain cracking; (b) three-dimensional channeling

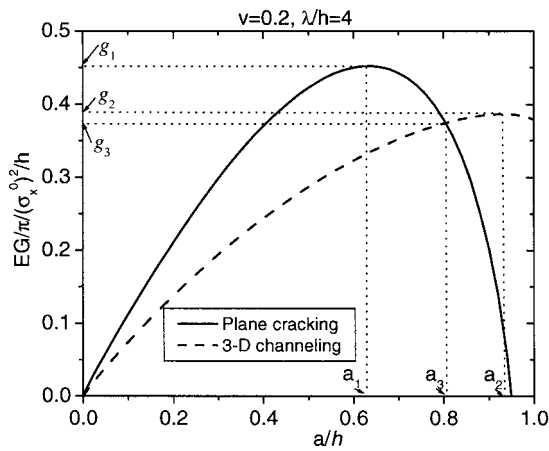


**Fig. 8.** Energy release rates for plane strain cracking and three-dimensional channeling

$$G = \frac{\sigma_x^0}{2a} \int_{h-a}^h \delta(y) dy = -\frac{\sigma_x^0}{a} \sum_{i=1}^N \frac{B_i h}{d_i} \sinh(c_i \lambda/h) \sin(d_i a/h) \quad (27)$$

Fig. 8 illustrates the energy release rates for plane strain cracking and 3D channeling. It can be seen that the local maximum energy release rates  $g_1$  and  $g_2$  exist at  $a_1$  and  $a_2$  for 2D cracking and 3D channeling, respectively. This is similar to the results of Beuth (1992) for a single crack and Shenoy et al. (2001) for periodic cracks. From this figure, one can see that when the crack depth is small, given a thermal loading the crack driving forces for both modes are small, and the crack will not initiate. If the thermal loading is so large that the driving force is larger than the fracture toughness, plane cracking will occur. Because the driving force increases with the crack depth for  $a < a_1$ , the cracking quickly propagates until the crack depth becomes larger than  $a_1$ . Thus, when the crack depth is smaller than  $a_1$ , the cracking is unstable. When  $a_1 < a < a_3$ , further loading is needed to make the crack to propagate toward the interface. Before  $a > a_3$ , because the crack driving force for plane strain cracking is larger than that for 3D channeling, the crack may stop within the overlay in the width direction. However, when  $a_3 \leq a$ , channeling cracks will propagate first under thermal loading. Thus, the crack will fully cross the overlay. With the increment of the loading, it is more difficult for cracks to propagate toward the interface, but as the stress in the overlay keeps increasing, a new crack will initiate and thus the stress will be relaxed again. It should be noted that Fig. 8 shows that the energy release rate for plane strain cracking is reduced to zero at  $a/h=0.95$ , whereas Beuth (1992) predicted it to be zero at  $a/h=1.0$ . This difference comes from the numerical truncations and the effect of the Poisson's ratio of the overlay.

## Conclusions and Future Work

An analytical model is proposed to investigate thermal cracking in asphalt overlaid rigid pavements. Using the boundary and loading conditions, one can obtain a series form solution for the elastic field. Comparisons of the solution with the FEM simulations show that the proposed model provides a good prediction of the elastic fields except for the neighborhood of the crack tip. Using this solution, the energy release rates can be calculated for plane strain cracking and 3D channeling. Comparing the energy release

rates with the fracture toughness of the overlay, one can predict the crack depth and crack initiation for a given temperature change.

In the current work, the material of the overlay is limited to linear elasticity. However, asphalt pavement materials typically exhibit viscoelastic behavior even at low temperatures. Thus, a viscoelastic constitutive model is ultimately needed. In addition, the temperature distribution in the thickness direction of the pavement varies along with the ambient temperature change, and thus the effect of a nonlinear temperature gradient needs to be further studied. Ultimately, field validation of the approach will be required. It should be noted that though this study is motivated by the thermal cracking in asphalt pavements and overlays, this method is applicable for other overlay/substrate structures such as protective coatings.

## Acknowledgments

This work is sponsored by Federal Highway Administration National Pooled Fund Study 776, whose support is gratefully acknowledged. The results and opinions presented herein are those of the writers and do not necessarily reflect those of the sponsoring agency. The writers would like to thank Professor John Hutchinson for his advice on the calculation of the energy release rates. The writers also thank Mr. E. Dave and A. Braham for their help in the preparation of the manuscript.

## References

- Beuth, J. L. (1992). "Cracking of thin bonded films in residual tension." *Int. J. Solids Struct.*, 29(13), 1657–1675.
- Bozkurt, D. (2002). "Three dimensional finite element analysis to evaluate reflective cracking potential in asphalt concrete overlays." Ph.D. dissertation, Univ. of Illinois at Urbana-Champaign, Ill.
- Bozkurt, D., and Buttlar, W. G. (2002). "Three-dimensional finite element modeling to evaluate benefits of interlayer stress absorbing composite for reflective crack mitigation." *Airport Technology Transfer Conf.*, Federal Aviation Administration, Atlantic City, N.J.
- Chen, G., and Baker, G. (2004). "Analytical model for predication of crack spacing due to shrinkage in concrete pavements." *J. Struct. Eng.*, 130(10), 1529–1533.
- Davids, W. G., and Turkiyyah, G. M. (1997). "Development of embedded bending member to model dowel action." *J. Struct. Eng.*, 123(10), 1312–1320.
- Freund, L. B., and Suresh, S. (2003). *Thin film materials: Stress, defect formation, and surface evolution*, Cambridge, New York.
- Fromm, H. F., and Phang, W. A. (1972). "A study of transverse cracking of bituminous pavements." *Asph. Paving Technol.*, 41, 383–423.
- Haas, R., Meyer, F., Assaf, G., and Lee, H. (1987). "A comprehensive study of cold climate airport pavement cracking." *Asph. Paving Technol.*, 56, 198–245.
- Hong, A. P., Li, Y. N., and Bažant, Z. P. (1997). "Theory of crack spacing in concrete pavements." *J. Eng. Mech.*, 123(3), 267–275.
- Huang, Y. H. (2003). *Pavement analysis and design*, Prentice-Hall, Englewood Cliffs, N.J.
- Huang, Z. H., Burgess, I. W., and Plank, R. J. (2003). "Modeling membrane action of concrete slabs in composite buildings in fire. I: Theoretical development." *J. Struct. Eng.*, 129(8), 1093–1102.
- Hutchinson, J. W., and Suo, Z. (1992). "Mixed mode cracking in layered materials." *Adv. Appl. Mech.*, 29, 63–191.
- Kim, J., and Buttlar, W. G. (2002). "Analysis of reflective crack control system involving reinforcing grid over base-isolating interlayer mixture." *J. Transp. Eng.*, 128(4), 375–384.

- Roque, R., Hiltunen, D. R., and Buttlar, W. G. (1995). "Thermal cracking performance and design of mixtures using superpave." *Asphalt Paving Technol.*, 64, 718–728.
- Shalaby, A., Abd, E. I., Halim, A. O., and Easa, S. M. (1996). "Low-temperature stresses and fracture analysis of asphalt overlays." *Transp. Res. Rec.*, 1539, 132–139.
- Shen, W., and Kirkner, D. J. (1999). "Distributed thermal cracking of AC pavement with frictional constraint." *J. Eng. Mech.*, 125(5), 554–560.
- Shenoy, V. B., Schwartzman, A. F., and Freund, L. B. (2001). "Crack patterns in brittle thin films." *Int. J. Fract.*, 109(1), 29–45.
- Timm, D. H., Guzina, B. B., and Voller, V. R. (2003). "Prediction of thermal crack spacing." *Int. J. Solids Struct.*, 40(1), 125–142.
- Xia, Z. C., and Hutchinson, J. W. (2000). "Crack patterns in thin films." *J. Mech. Phys. Solids*, 48(6–7), 1107–1131.
- Waldhoff, A. S., Buttlar, W. G., and Kim, J. (2000). "Investigation of thermal cracking at Mn/ROAD using the Superpave IDT." *Asph. Paving Technol.*, 45, 228–259.
- Yang, Y. B., and Lin, B. H. (1995). "Vehicle-bridge interaction analysis by dynamic condensation method." *J. Struct. Eng.*, 121(11), 1636–1643.
- Yin, H. M., Buttlar, W. G., and Paulino, G. H. (2005) "A two-dimensional elastic model of pavements with thermal failure discontinuities." *Proc., 3rd MIT Conf. Comput. Fluid Solid Mech.*, Elsevier, Oxford, U.K., 539–542.
- Zhang, T. H., and Huan, Y. (2004). "Substrate effects on the micro/nanomechanical properties of TiN coatings." *Tribol. Lett.*, 17(4), 911–916.